RSC Advances

PAPER

View Article Online
View Journal | View Issue

Cite this: *RSC Adv.*, 2024, **14**, 37570

Facile assembly of flexible humidity sensors based on nanostructured graphite/zinc oxide-coated cellulose fibrous frameworks for human healthcare†

Zaka Ullah, *[a] Ghulam M. Mustafa,[a] Ali Raza,[a] Adnan Khalil,[b] Aboud Ahmed Awadh Bahajjaj,[c] Rashida Batool,[d] Nazmina Imrose Sonil,[e] Irfan Ali[f] and Muhammad Faizan Nazar[d]

The development of flexible, cost-effective, highly efficient, and reliable humidity monitoring sensors is in high demand owing to their wide-range of applications in industrial domains. In this study, a humidity sensor was fabricated based on graphite/zinc oxide nanoparticle (G/ZnO-NP)-coated cellulose paper. A bar device was designed using computer software, and its sketch was printed on cellulose paper, with graphite bars then added using the pencil-drawing method, and then ZnO-NP paste was coated on the graphite patterns. Scanning electron microscopy and X-ray diffraction analysis were used to respectively inspect the morphological and structural features of the samples. For sensor fabrication, copper wires were attached to the electrodes using copper tape. The fabricated device was placed into a chamber with varying relative humidity (RH) levels of 11%, 24%, 43%, 62%, 84%, and 97%, controlled using the salt solutions inside the chamber. The response of the sensor was recorded in terms of the change in resistance of the device upon exposure to different humidity environments. The sensor delivered a response time as short as 4.31 s for the 24% RH condition, and a recovery time as short as 10.05 s for 43% RH. Moreover, the sensor exhibited a sensitivity of 717% for the 97% RH condition. The sensor was also evaluated for human breath monitoring, showing distinctive responses for inhalation and exhalation.

Received 8th August 2024
Accepted 11th November 2024

DOI: 10.1039/d4ra05761a

rsc.li/rsc-advances

1 Introduction

There is increasing interest in the facile assembly of cost-effective ultrasensitive humidity sensors due to the rising demand for them in a diversity of emerging applications.[1] Flexible and environmentally friendly sensors have been demonstrated that can easily be integrated into many desired places.[2,3] Carbon materials are playing a revolutionary role in this scenario, particularly due to their flexibility and stretchability.[4,5] As one key such material, graphite possesses high electrical conductivity, good mechanical strength, and suitable chemical properties, which make it a popular choice for the fabrication of sensors.[6] Moreover, the layers in layered graphite are coupled to one another by weak van der Waals forces of attraction, in which the electrons are delocalized due to the small energy gap between the valence and conduction bands; this makes graphite an excellent conductor. Although graphene and carbon nanotubes can be superior to graphite, their preparation is rather complicated and expensive.[7]

Water vapor in air is essential for life on earth but can affect the comfort level of living things. Beyond such typical significance, humidity also plays a major role in the operation of different electronic circuits, electrostatic components, and high-voltage devices.[8] It is the key factor to be monitored in food storage, agricultural environments, weather-casting, and in a variety of aspects in the pharmaceuticals, mining, manufacturing, and automobile industries.[1,9] For this purpose, optical, surface acoustic wave, field-effect transistor, magnetic, thermal, and resonance-based humidity sensors have been demonstrated.[10] Moreover, cellulose paper, textiles, plastic, and rubbers have extensively been used as flexible substrates. Such

[a]*Department of Physics, Division of Science and Technology, University of Education, Lahore 54770, Pakistan. E-mail: zaka.ullah@ue.edu.pk*

[b]*Institute of Physics, Khwaja Fareed University of Engineering and Information Technology, Rahim Yar Khan 64200, Pakistan*

[c]*Department of Chemistry, College of Science, King Saud University, Riyadh 11451, Saudi Arabia*

[d]*Department of Chemistry, Division of Science and Technology, University of Education, Lahore 54770, Pakistan*

[e]*State Key Laboratory of Radio Frequency Heterogeneous Integration, College of Electronics and Information Engineering, Shenzhen University, Shenzhen 518060, China*

[f]*Physics Characterization and Simulations Lab (PCSL), Department of Physics, School of Natural Sciences (SNS), National University of Sciences and Technology (NUST), Islamabad 44000, Pakistan*

† Electronic supplementary information (ESI) available. See DOI: https://doi.org/10.1039/d4ra05761a

substrates are more effective, lightweight, and cost-effective, and provide periodic elasticity and bendability to tolerate the applied stress or strain more efficiently compared to other substrates, such as hard silicon or conventional semiconductors. In particular, cellulose paper is often preferred to others as it is highly flexible, cost-effective, bio-degradable, and customizable in shape and size.[1,10,11]

Humidity sensors, also known as hygrometers, are generally classified into two main categories, namely resistive and capacitive, based on their design, beyond which resistive sensors could be impedance or conductance based as per their sensing mechanism.[12] Efficient humidity sensors offer accurate measurement, high sensitivity, fast response, long-term reliability and response stability, consistency, and temperature compensation. In addition to these features, researchers are trying to address their limited temperature and humidity range, poor hysteresis, contamination, high power consumption, high cost, device complexity, size suitability, and facile integration of the sensor to make them more versatile and reliable for many desired applications.[13] Furthermore, their inflexibility, poor selectivity, weak mechanical and chemical stability, ordinary electrical, mechanical, and stretching characteristics, harmfulness to the environment, complex structures, and high-technology instrument-based fabrication are some of the major limitations of the current humidity sensors. A way to concurrently convert all these drawbacks into shining features of a single device is one of the key challenges for researchers working in this research realm. Ongoing attempts are being made to overcome these challenges by using different combinations of active materials or by employing advanced methodologies for fabrication. The fundamental motives for these flaws are also associated with the limited understanding of the devices for their use in a variety of target applications.[1,2]

Researchers have reported the assembly of nanomaterial-based electrodes with unusual stability, acceptable porosity, suitable crystalline structure, exceptional surface area, intensive adsorption capabilities, and admirable low toxicity for diverse applications.[11,14,15] Such properties offer valuable characteristics to humidity sensors. Materials based on zinc oxide (ZnO) nanoparticles have attracted substantial interest in a diversity of fields owing to their extraordinary capability to capture charge carriers, allowing successful doping with various carbon materials and transition metals. ZnO nanostructures can deliver a notable response for humidity sensors. This metallic oxide is hydrophilic and offers the excellent adsorption of water molecules on its surface. This interesting characteristic has unfolded new paths for the investigation and application of ZnO-based nanomaterials for humidity sensing. Hydroxyl and oxygen absorption defects on ZnO surfaces have effective hydrophilicity while oxygen vacancy defects can also boost the dissociation process of water molecules to enhance the response time of the sensors. Furthermore, the large surface area can offer excessive sites for water molecule adsorption, which can impressively improve the sensor response. All these valuable features suggest ZnO's great potential as a material for humidity sensors.[16–20]

The prior literature shows some prior work in this field, including a report on the fabrication of flexible humidity sensor based on pencil-drawn graphite patterns. In that study, a 10B pencil was used for graphite coatings and the sensor was evaluated for the detection of human breath. However, the sensor delivered a poor, unstable, and slow response. Moreover, the sensitivity of the sensor was limited and there was no estimation of the cycling performance of the sensor.[21] Another similar study demonstrated a humidity sensor based on chemically pretreated pencil graphite. A 2B pencil was used for graphite coating; however, the sensitivity of the sensor was limited and its response was also slow and poor. Moreover, there was no sufficient real-time or cycling performance evaluation of the sensor performed in that study.[22] Researchers also fabricated a pencil-drawn graphite-based capacitive humidity sensor on a novel wood substrate. While the design of the device had some novelty and simulations were performed to reveal the capacitance characteristics of the device. However, the device size was not convenient, the response was less stable than desired, and the sensitivity, response time, and recovery time were poor, while the cycling durability was not evaluated.[23] Beyond pencil-drawn graphite-based humidity sensors, it was reported in another study that sensors based on only ZnO nanomaterials delivered a large response and recovery time, and low sensitivity.[24]

To further advance the applications of pencil-drawn graphite patterns on flexible substrates for humidity sensing, here we demonstrated a humidity sensor that addresses all the aforementioned concerns and fulfills the demands for facile, low-price, and fast fabrication of sensors. The use of a 2B pencil and ZnO-NPs improved the sensitivity of the sensor. The integration of ZnO-NPs with graphite patterns endowed the sensor with a faster and stable response, which has been absent so far in graphite-based humidity sensors. The design and assembly of the sensor were flexible and customizable for different shapes and sizes. All these features contribute to a real-time response and cycling durability of the demonstrated sensor. Moreover, the pencil-drawing method offers a simple and facile way for the deposition of graphitic structures on appropriate substrates, making use of easily available and less expensive graphite pencils. This method additionally permits the formation of desired patterns on cellulose paper. Likewise, ZnO nanoparticles paste was coated on the graphite bar device through an extremely simple doctor blade method. The sensor with all these advantages delivered a fast and distinctive response, together with ultrasensitivity and notable mechanical stability. The sensor was also evaluated for human breath monitoring. The prepared electrodes and fabricated devices involve quite simple, time-saving, less expensive, and environmentally friendly methodologies, which could be of great significance for the fabrication of different flexible electronic devices and high-performance humidity sensors.

2 Experimental

A bar device sketch was designed using computer software, and printed on conventional A4 printing paper mainly consisting of cellulose fibers. Graphite coating was applied on the paper as per the printed design through the direct pencil-drawing

method. To optimize these graphite electrodes, 2B, 4B, 6B, 8B, and 10B pencils were used. The uniformity in graphite coatings was achieved by repeating the same number (10) of pencil strokes over the desired area for all the prepared samples. Afterward, a paste of ZnO nanoparticles that were purchased from Sigma-Aldrich, USA, was prepared in deionized water and its coating was applied on graphite electrodes using the doctor blade method. Resistance measurements of the electrodes were performed five times, and the average resistance values were considered. Scanning electron microscopy (SEM) micrographs were obtained on a Nova Nano Scanning Electron Microscope, and an X-ray diffractometer (German, D8 Advance, Germany) was used to acquire the X-ray diffraction (XRD) patterns. ImageJ software was used to determine the sizes of the micro- and nanostructures in the SEM images. Copper wires were attached to the two electrodes of the device using copper tape. The assembly of the sensor is depicted in Fig. 1a.

The evaluation of the sensor was performed by varying the relative humidity (RH) environments in beakers (considered as humidity chamber) as 11%, 24%, 43%, 62%, 84%, and 97%, obtained through the application of salt solutions of LiCl, CH_3COOK, K_2CO_3, $CuCl_2$, KCl, and K_2SO_4, respectively. When certain salt solutions are placed in closed environments, there is a specific concentration of water vapors both inside the solution and in the surrounding air. These solutions absorb or desorb water vapor in the environment to reach the equilibrium state. The process depends on the relative humidity (RH) of the environment. Each salt solution has a specific equilibrium relative humidity at a given temperature, at which point the solution neither gains nor loses water vapor; for instance, a saturated solution of potassium chloride (KCl) maintains an RH of ~84% at 25 °C, which means that the water vapor in air will remain constant and the humidity level will be maintained. Based on this principle, saturated salt solutions are frequently used to maintain the desired humidity levels in closed environments.[25,26] The same procedures and schemes were used in the demonstrated study to produce the humidity levels of 11%, 24%, 43%, 62%, 84%, and 97% using the salt solutions of LiCl, CH_3COOK, K_2CO_3, $CuCl_2$, KCl, and K_2SO_4, respectively.

The deviations in these RH levels were found to be up to ±3%. The fabricated sensor was connected to a Keithley 2400 Source Meter and a commercial humidity gauge was adjusted inside the chamber to confirm the actual humidity values. The sensor was placed in the beakers with different relative humidity environments for a short time, and then brought outside the beaker, and the effects of humidity on the sensor were recorded. The sensing setup is illustrated in Fig. 1b. All the humidity response experiments were performed at ~25 ± 2 °C.

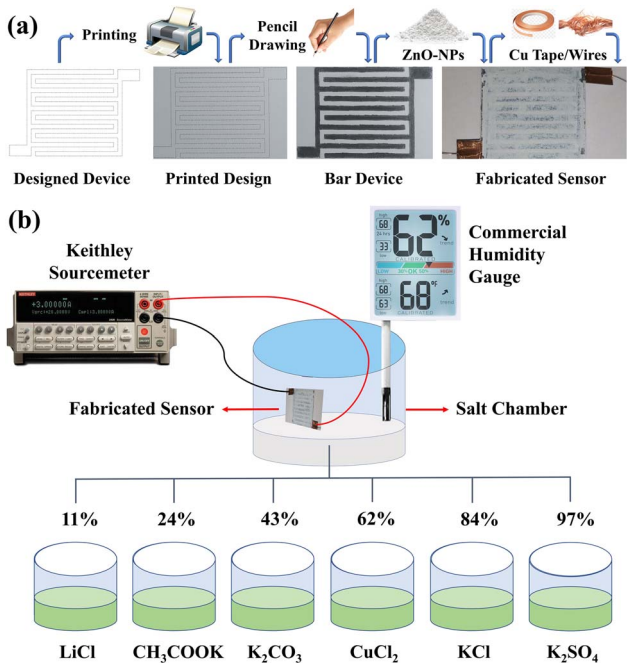

Fig. 1 (a) Digital photographs and illustrations showing the fabrication of the G/ZnO-NP-based humidity sensor. (b) Sensing setup for the humidity sensor.

3 Results and discussions

Fig. 2a depicts the SEM micrograph of the graphite-coated cellulose paper. Most area of the pencil-drawn graphite film was smooth and thoroughly covered the substrate. However, there were also some rough areas, and the graphite film was decorated with micro- and nano-scale graphitic structures. The graphite structures were produced during the repetitive pencil strokes on the cellulose paper. Frictional force caused traces of graphite to be broken off the pencil core during the movement of the pencil, which were subsequently deposited on the surface of the substrate. Most of the traces settled down to the substrate surface to form the graphite coating; however, some could not get adjusted and stayed on the graphite coating. These structures included nanoparticles, with two sized 47 and 89 nm indicated by the arrows in Fig. 2a. Fig. 2b shows the ZnO-NPs coating above the graphite bars on cellulose paper. It is obvious from the image that the ZnO-NPs were agglomerated and it is hard to find the sharp boundaries of individual ones. This could also be attributed to the coating methodology as this involved the formation of a paste of ZnO-NPs. Yet, a few spots refer to such individual nanoparticles where the concentration of the material was low, as shown by the yellow arrows in the figure. It is also important to mention that such a morphology of ZnO-NPs coating is important to enhance the conducting paths in the sensing material, particularly if the substrate is flexible. The micro- and nanostructures of graphite along with ZnO-NPs enhance the electrical stability of the device.

Fig. 2c shows the diffraction pattern of the pencil-drawn graphite coating on cellulose paper. A hump-like broad peak could be observed at a 2θ value of 15.24°, which was attributed to the amorphous paper substrate. The fingerprint peak of graphite was recorded at a 2θ value of 26.23° (d-spacing: 3.3950 Å, space group: $P6_3mc$ (186), crystal structure: hexagonal), which matched with JCPDS card no. 75-1621 and was indexed as the 002 plane. All the other obvious peaks in the pattern could be ascribed to the binder in the form of metallic oxides in the graphite pencils. The diffraction peaks observed at 2θ values of 22.36°, 29.26°, 38.98°, 48.24°, 54.45°, 60.32°, and 64.12° were

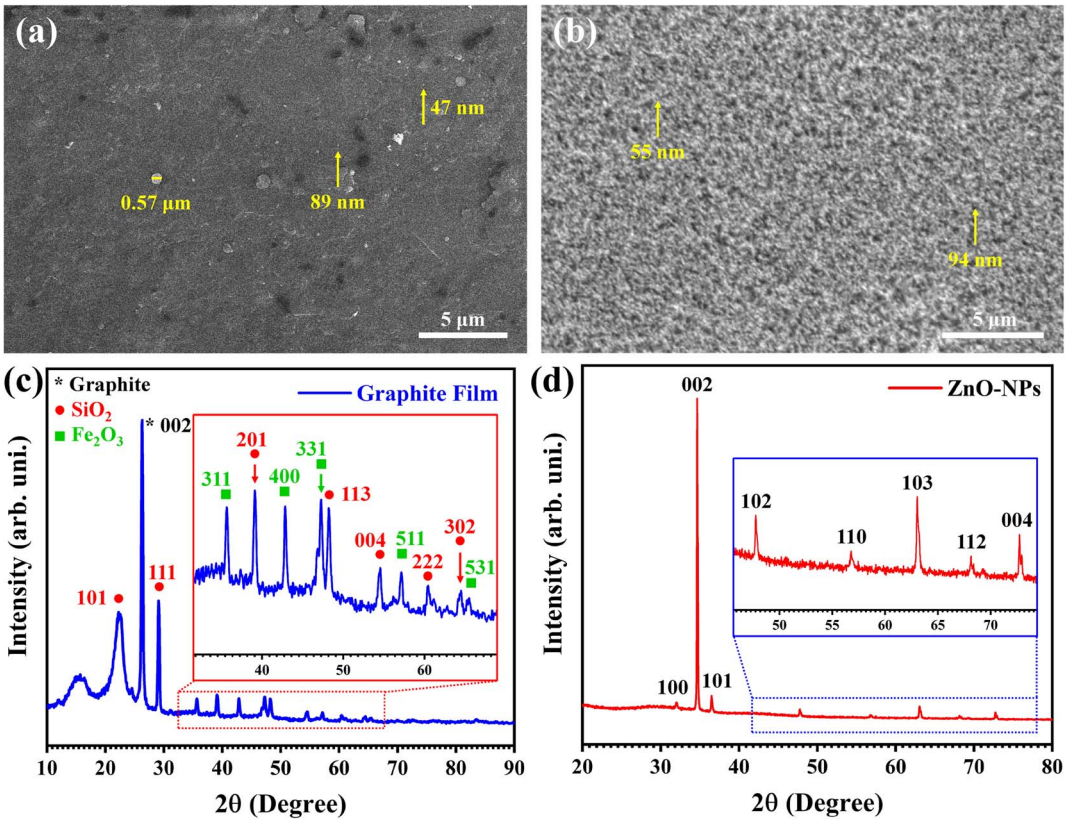

Fig. 2 SEM micrographs showing the surface morphologies of (a) graphite and (b) graphite/ZnO-NPs coating on cellulose paper. XRD patterns of (c) pencil-drawn graphite and (d) ZnO-NPs coating on cellulose substrate.

respectively assigned to the 101, 111, 201, 113, 004, 222, and 302 planes for SiO_2 as per JCPDS card no. 82-1235 (space group: $P4_12_12$ (92), crystal structure: tetragonal). The remaining peaks found at 2θ values of 35.56°, 42.88°, 47.23°, 57.05°, and 65.53° were respectively indexed to the 311, 400, 331, 511, and 531 planes for Fe_2O_3 as per JCPDS card # 75-0033 (space group: $Fd\bar{3}m$ (227), crystal structure: cubic). These outcomes were in good agreement with the reported literature for pencil-drawn graphite films.[27]

The major peak in the ZnO diffraction pattern was observed at 2θ as 34.71°, which was assigned to the 002 plane as per JCPDS card No. 36-1451 (space group: $P6_3mc$ (186), crystal structure: hexagonal). All the other small peaks are also matched with this standard data. Consequently, the peaks at 2θ values of 31.96°, 36.44°, 47.78°, 56.85°, 63.08°, 68.14°, and 72.72° were respectively attributed to the 100, 101, 102, 110, 103, 112, and 004 diffraction planes, as shown in Fig. 2d. The observations of the diffraction peaks were also consistent with the already reported data in the literature.[28]

Fig. 3a shows the responses of the fabricated humidity sensors based on G/ZnO-NPs coatings with graphite coatings employed using 2B, 4B, 6B, 8B, and 10B pencils. The fabricated sensors were evaluated for RH levels from 11% to 97%. It could be observed that the resistance of the sensor decreased with the increase in RH level, and this decrease was more significant when the graphite pencil changed from 10B to 2B. For the 2B pencil, the resistance decreased from 7.28 to 1.04 GΩ, and for the 10B pencil, the resistance decreased from 905 to 413 MΩ with the increase in RH level from 11% to 97%. The difference in resistance change rate could be attributed to the fact that the initial resistance of the graphite pencils increased from 10B to 2B owing to the decrease in graphite concentration in the pencils. It was interesting to note that the final resistance values of each sample at 97% RH were comparable, which could be ascribed to the maximum effect of the water molecules. This effect was comparable in all the samples as the concentration of water molecules (humidity) was comparable at the same RH as 97%. The 2B pencil was found to be most appropriate, as a greater change in the resistance of the sensor will offer a higher sensitivity. Consequently, further measurements were performed with sensors in which graphite coatings were employed using the 2B pencil. In addition, five devices were fabricated using this pencil, and their response to varying RH levels was recorded to further assess the reproducibility of the devices, as depicted in Fig. S1 (ESI).† It could be observed that the responses of all the devices were consistent and comparable. Moreover, Table S1† in the ESI† shows that the standard deviation of the response was not more than 0.60, which signifies the notable reproducibility and significant reliability of the results.

The deposition of graphite was meticulously executed to ensure the uniform distribution across the surface of cellulose paper. Since, applying a graphite coating directly onto the graphite layer was ineffective, the thickness of the graphite layer remained comparable across the sample surface. Fig. 3b

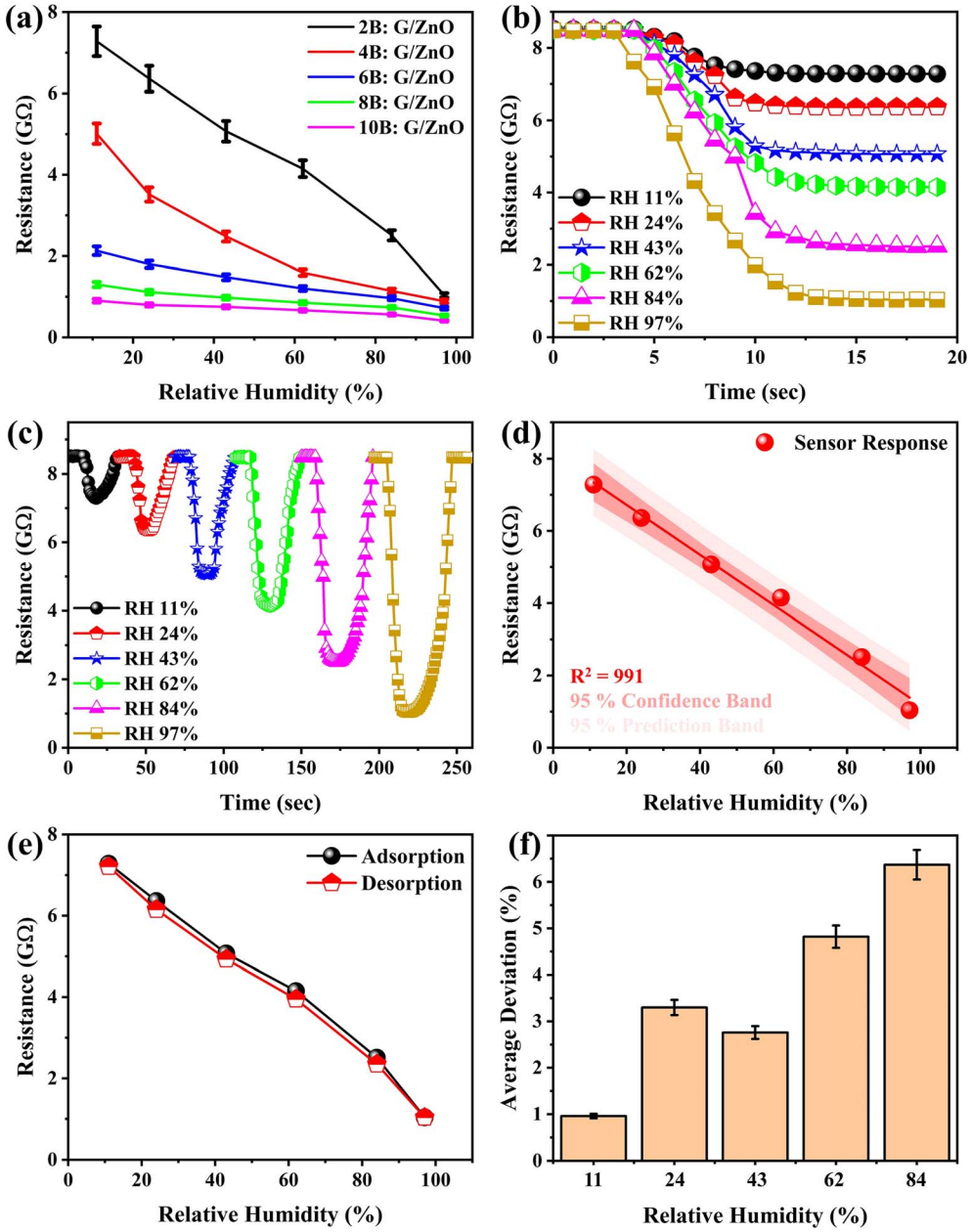

Fig. 3 Response of the sensor upon varying the humidity between 11% and 97%: (a) for sensors based on ZnO-NPs coated-graphite bar devices fabricated using graphite pencils of different grades; (b) when the sensor was brought inside the chamber and kept there for some time; (c) when the sensor was brought inside the chamber and then immediately taken out of the humid environments; (d) linearly fitted maximum response of the sensor; (e) response hysteresis for absorption followed by subsequent desorption; (f) average deviations in response during the hysteresis measurements.

illustrates the responses of the sensor when it was just put into the chambers with different RH levels, and kept there for some time. It could be noted that the change in resistance increased with the increase in RH level, and remained almost constant when the sensor remained inside the chamber. The resistance changed from 8.53, 8.50, 8.50, 8.50, 8.48, and 8.49 GΩ to 7.28, 6.36, 5.07, 4.15, 2.51, and 1.04 GΩ as the humidity was changed as 11%, 24%, 43%, 62%, 84%, and 97%, respectively. Moreover, when the sensor was brought into the environments with different RH levels, and then immediately taken out of the chamber, there was still a significant response of the sensor to the different RH levels, as depicted in Fig. 3c. The sensing was performed for RH levels as 11%, 24%, 43%, 62%, 84%, and 97%. It is obvious from the figure that the sensor showed efficient recovery after it was taken out of the environments with higher RH levels.

The resistance of the sensor decreased linearly as the RH level increased, with a notable linearity (R^2) of 991, as given in Fig. 3d. It could also be observed that the sensor offered distinctive selectivity for all the provided RH levels. The response hysteresis was recorded for the demonstrated sensor, as this plays a crucial role in the evaluation of the performance

of humidity sensors. During the measurements, the sensor was exposed to varying RH levels and its response was recorded; first, the RH level was increased from 11% to 97%, during which water vapors were adsorbed on the surface of the sensor, and subsequently, the RH level decreased from 97% to 11%, during which the water vapors were desorbed from the surface of the sensor, forming a loop of the sensor response, as depicted in Fig. 3e. The loop with a minimal area signified the high performance of the demonstrated humidity sensor. Small deviations in response of 0.96%, 3.30%, 2.76%, 4.82%, and 6.37% were found, respectively, at RH levels of 11%, 24%, 43%, 62%, and 84%, as shown in Fig. 3f. These deviations could be attributed to the wettability of the sensor as it took some time for full recovery.[29]

The sensitivity of the fabricated sensor was determined at different RH levels using the following equation:[30]

$$S = \left(\frac{R_i - R_{RH}}{R_i}\right) \times 100$$

where S is the sensitivity, R_i is the initial resistance, and R_{RH} is the resistance of the sensor at a particular RH level. It was calculated as 17%, 34%, 68%, 105%, 241%, and 717%, respectively, for RH levels of 11%, 24%, 43%, 62%, 84%, and 97%, as given in Fig. 4. Moreover, the figure also depicts the increase in weight of the sensor with increasing the RH level, as a greater amount of water vapors is adsorbed by the sensor at higher RH levels, which increase its weight. At 11% RH, the weight of the device increased by ~2.2%, and by ~22.8% when the provided RH level was 97%. This further confirmed the significant absorption of water molecules on the surface of the sensor in humid environments.[31]

Fig. 5a shows the determination of the response and recovery time of the sensor for a RH level of 62%. Typically, the response time is considered as the time during which a change in resistance is observed from 10% to 90%, and the recovery time is considered as the time during which the change in resistance is recorded from 90% to 10%, as depicted in the figure. The response and recovery time of the sensor for a RH level of 62% were respectively recorded as 5.74 and 10.13 s. The delivered response and recovery times were quite efficient compared to those of many humidity sensors reported in the literature. Moreover, these well meet the criteria of such sensors for a diversity of practical applications, including human health monitoring, food processing, and agricultural gadgets. Fig. 5b shows the response and recovery time of the demonstrated humidity sensor for all the investigated RH levels. The response time was measured as 4.64, 4.31, 4.49, 5.74, 5.96, and 6.68 s, and the recovery time as 10.41, 10.93, 10.05, 10.13, 12.33, and 13.87 s for RH levels of 11%, 24%, 43%, 62%, 84%, and 97%, respectively.

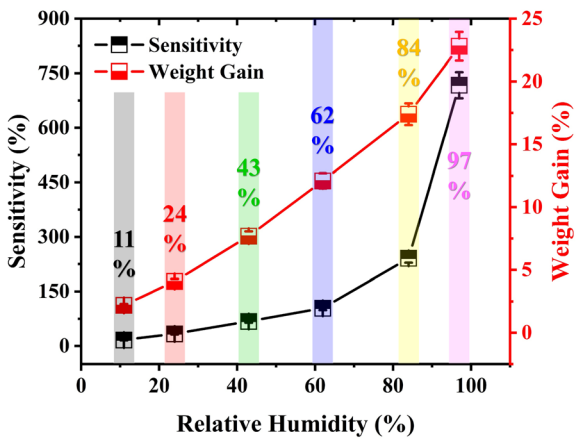

Fig. 4 Sensitivity and weight gain of the sensor in response to the increasing RH level.

Long-term stability is one of the crucial features of humidity sensors for their practical applications. Hence, the stability of the demonstrated sensor was evaluated by measuring its response to various RH levels for 10 days. The sensors were kept in humid environments and their responses were recorded once a day, as depicted in Fig. 5c. It is obvious that the responses of the sensors were highly stable, and showed minimal degradation over the 10 days, with degradations in response of only 0.41%, 0.63%, 1.38%, 2.65%, 5.60%, and 6.25%, respectively, for RH levels of 11%, 24%, 43%, 62%, 84%, and 97%. Notably, the effect of the humid environment became stronger with the increase in RH level. However, the results evidence the high stability of the sensors, and their suitability and feasibility for practical applications. Table 1 shows the performance comparison of the demonstrated humidity sensor with that of other sensors reported recently in the literature.

For practical applications of the demonstrated humidity sensor in human health monitoring, the sensor was integrated inside a surgical mask, as depicted in the insets of Fig. 5d. The upper layer of a multi-layer mask was cut and the sensor was fitted inside it. This was barely visible from the outside, as shown by the digital photograph. The wires were then connected to a circuit, and the mask was worn by a volunteer. The process of breathing changes the humidity around the mouth of the volunteer, and the surface of the sensor, which was open to the environment around the mount, was exposed to these humidity changes. As these changes were significantly higher during inhalation and exhalation, the response signal delivered sufficient changes in the resistance of the sensor, as displayed in Fig. 5d. Moreover, the response signal remained sharp and stable, which also evidenced the proficiency of the demonstrated sensor for human breath detection. If a patient was suffering from any disease, the breath response of the sensor could be different as per the chemical species in the breath of the patient. In this scenario, further calibrations of the breath could be performed for the detection of diseases in this patient, and the sensor could thus be employed for human healthcare.

The sensing mechanism of graphite on cellulose paper is associated with hydrophilic functional groups present on its surface. When humidity is increased and water molecules come in contact with the sensor, the hydroxyl groups (OH^-) from water molecules are absorbed on the surface of the sensor. The conductivity of the active material increases due to the initiation of electron transfer from the active material to the hydroxyl groups.[40,41] A similar situation has been found for ZnO nanoparticles layer; whereby, owing to the n-type nature and higher

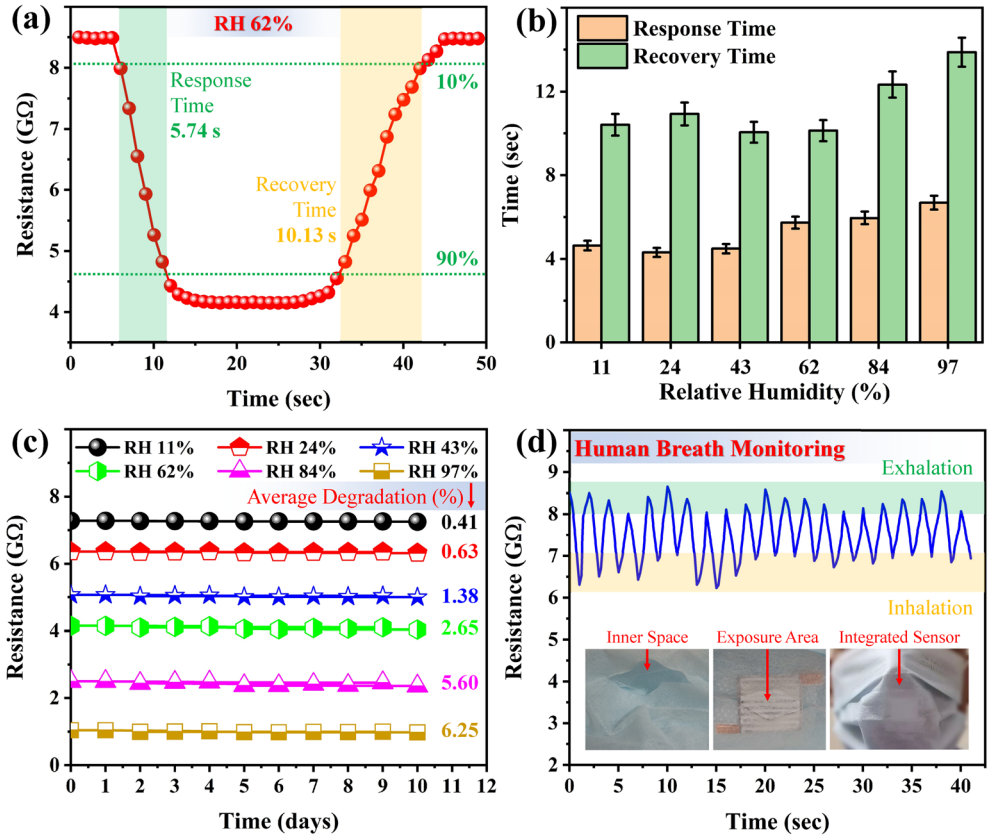

Fig. 5 Response and recovery time of the demonstrated sensor for (a) 62% RH, and (b) all the studied RH levels. Evaluation of the sensor for its (c) stability in humid environments, and (d) human breath monitoring.

Table 1 Resistive humidity sensor performance comparison of the demonstrated sensor with other sensors recently reported in the literature, in terms of RH range (%), response and recovery time, and sensitivity

Sensing material	RH range (%)	Response time (s)	Recovery time (s)	Sensitivity (%)	Ref.
PVA/graphene	10–80	11	35	66.4	32
Cellulose/graphene	15–99	45	33	42	33
Ag-NP/graphene QDs	25–95	15	15	98.14	34
CNTs/CNFs	11–95	276	211	61.5	35
PDDA/rGO	11–97	147	133	37.43	36
MoS_2/Si-NWs	11–95	26.4	15.1	392	37
rGO/ZnO/Cu	11–97	19	42	97.79	38
Carbon/ZnO	11–84	17.4	32.1	96	16
Rice paper	0–100	5	16	97	39
Graphite/ZnO	**11–97**	**4.31**	**10.05**	**717**	**This work**

electron-transfer ratio, the resistance of the ZnO layer is decreased. The hydrophilic functional groups are then adsorbed on the surface of ZnO layer and increase the concentration of free elections, which ultimately lowers the resistance of the active material. Furthermore, in dry conditions, the electrons cannot easily transfer to their neighboring (carbon and ZnO) atoms through a tunneling effect. However, after the absorption, the hydroxyl groups and water molecule membranes on the surface produce pathways for electron transport, which decreases the resistance of the sensor. This effect is more significant with an increase in RH level. Thus, the resistance of the device decreases with the increase in RH level.[16,17]

In a case when the RH level is decreased, the water molecules are desorbed from the surface of the sensor, and the resistance of the device starts increasing. It is interesting to mention here that the increase or decrease in the resistance of the sensor is generally associated with the pristine resistance of the device. Devices with lower resistance may offer an increase in resistance upon an increase in RH level, while devices with higher resistance may offer a decrease in resistance upon an increase in RH level, as was observed in the current scenario. Devices

that can deliver greater change in resistance upon a change in RH level have higher sensitivity, and these are desired in a wide range of practical applications. It could be seen from Table 1 that the demonstrated sensor offered a valuable response to changes in humidity, and can be employed in practical applications, including food processing, agriculture, pharmaceuticals, human healthcare, meteorology, and microelectronics.

In the future, sensors based on stretchable substrates may be demonstrated, which will improve the flexibility of the devices and endow the sensors with stretchability. The use of textile/fabric substrates may enhance the mechanical properties of the sensors and will make them suitable for proficient integration into human clothes to offer smart health monitoring. Moreover, advanced materials may be designed to deliver a stable response to varying temperature environments. In particular, auspicious nanomaterials can be employed for human health treatments.[42] In this scenario, detailed studies conducted on the human body with diverse scopes could benefit from employing advanced sensors for human safety,[43] with special attention given to the performance of such sensors for the detection of diseases. The engineering of sensing materials may furnish the humidity sensors with higher sensitivity and selectivity for sundry diseases, which will enhance their scope in human healthcare. In addition, the sensors can be equipped with wireless charging mechanism and their applications can be extended to food monitoring for better assuring human health anxieties.[44]

4 Conclusions

A facile fabrication of a humidity sensor based on graphite/ZnO nanoparticles-coated conventional cellulose paper was realized in this work. SEM and XRD analyses of the samples were performed. The humidity sensor was assembled by simply connecting copper wires along two edges of the bar device using copper tape. The sensor demonstrated a remarkable response to changes in the RH levels as 11%, 24%, 43%, 62%, 84%, and 97%, which were obtained using salt solutions of LiCl, CH_3COOK, K_2CO_3, $CuCl_2$, KCl, and K_2SO_4, respectively. The sensor delivered the shortest response time of 4.31 s for a RH level of 24%, and the shortest recovery time as 10.05 s for a RH level of 43%. The sensor showed a hysteresis loop with a negligible area, and the maximum deviation in adsorption/desorption was recorded as 6.37% for a RH level of 84%, which suggests the high efficiency of the demonstrated humidity sensor. Moreover, the sensor showed an ultrasensitivity of 717% for 97% RH. The sensor was also assessed for human breath monitoring, and its response remained sharp and stable during inhalation and exhalation, evidencing its high performance for many desired practical applications, including human healthcare.

Data availability

Data are available from the authors upon reasonable request.

Author contributions

Zaka Ullah: conceptualization, data curation, investigation, methodology, resources, software, validation, writing – original draft. Ghulam M. Mustafa: formal analysis, resources, software, writing – review & editing. Ali Raza: formal analysis, software, writing – review & editing. Adnan Khalil: formal analysis, funding acquisition, writing – review & editing. Aboud Ahmed Awadh Bahajjaj: formal analysis, funding acquisition, project administration, resources, writing – review & editing. Rashida Batool: formal analysis, software, visualization. Nazmina Imrose Sonil: formal analysis, software, writing – review & editing. Irfan Ali: methodology, resources. Muhammad Faizan Nazar: formal analysis, funding acquisition, project administration, resources, supervision.

Conflicts of interest

The authors declare that they have no known competing financial interests or personal relationships that could have appeared to influence the work reported in this paper.

Acknowledgements

This work was funded by the Researchers Supporting Project Number RSPD2024R763, King Saud University, Riyadh, Saudi Arabia.

References

1 T. Delipinar, A. Shafique, M. S. Gohar and M. K. Yapici, Fabrication and Materials Integration of Flexible Humidity Sensors for Emerging Applications, *ACS Omega*, 2021, **6**(13), 8744–8753.
2 L. Ma, R. Wu, A. Patil, S. Zhu, Z. Meng, H. Meng, *et al.*, Full-Textile Wireless Flexible Humidity Sensor for Human Physiological Monitoring, *Adv. Funct. Mater.*, 2019, **29**(43), 1904549.
3 Y. Lv, J. Wei, Z. Huang, Z. Zhang, S. Ding, C. Zhang, *et al.*, Superelastic bamboo fiber-based spongy aerogel for flexible piezoresistive sensors with wide response range and high sensitivity, *Chem. Eng. J.*, 2024, **488**, 151053.
4 T. Q. Trung, L. T. Duy, S. Ramasundaram and N.-E. Lee, Transparent, stretchable, and rapid-response humidity sensor for body-attachable wearable electronics, *Nano Res.*, 2017, **10**(6), 2021–2033.
5 B. Xie, Y. Guo, Y. Chen, H. Zhang, J. Xiao, M. Hou, *et al.*, Advances in Graphene-Based Electrode for Triboelectric Nanogenerator, *Nano-Micro Lett.*, 2025, **17**(1), 17.
6 S. S. Annu, R. Jain and A. N. Raja, Review—Pencil Graphite Electrode: An Emerging Sensing Material, *J. Electrochem. Soc.*, 2020, **167**(3), 037501.
7 Q. Li, Z. Ullah, W. Li, Y. Guo, J. Xu, R. Wang, *et al.*, Wide-Range Strain Sensors Based on Highly Transparent and Supremely Stretchable Graphene/Ag-Nanowires Hybrid Structures, *Small*, 2016, **12**(36), 5058–5065.

8 P. Li and F. Yang, Preparation and performance of TiO_2/ZnO humidity sensor based on TiO_2, *Mater. Sci. Eng. B*, 2023, **298**, 116902.
9 N. Mohamadbeigi, N. Rafiefard, F. Ejehi, R. Mohammadpour and A. Iraji zad, Triboelectric Nanogenerator-Enabled 3D Microporous Polydimethylsiloxane–Graphene Oxide Nanocomposite for Flexible Self-Powered Humidity Sensing Applications, *Energy Technol.*, 2024, **12**(3), 2301136.
10 Y. Dou, C. Li, W. Luo, L. Qian, L. Wang, D. Li, *et al.*, Surface acoustic wave relative humidity sensor based on GO/TiO_2 sensitive film, *Sens. Actuators, A*, 2024, **365**, 114906.
11 A. M. Ramesh, M. Rajesh, A. Chandran and K. P. Surendran, Gold-Nanoparticle-Based Flexible Humidity Sensor for Breath Monitoring and Smart Irrigation Systems, *ACS Appl. Nano Mater.*, 2024, **7**(13), 15593–15605.
12 H. Farahani, R. Wagiran and M. N. Hamidon, Humidity Sensors Principle, Mechanism, and Fabrication Technologies: A Comprehensive Review, *Sensors*, 2014, **14**(5), 7881–7939.
13 K. B. Arman, Recent Studies on the Humidity Sensor: A Mini Review, *ACS Appl. Electron. Mater.*, 2022, **4**(10), 4797–4807.
14 Y. Wang, Y. Xu, W. Zhai, Z. Zhang, Y. Liu, S. Cheng, *et al.*, In-situ growth of robust superlubricated nano-skin on electrospun nanofibers for post-operative adhesion prevention, *Nat. Commun.*, 2022, **13**(1), 5056.
15 V. Montes-García and P. Samorì, Humidity Sensing with Supramolecular Nanostructures, *Adv. Mater.*, 2024, **36**(12), 2208766.
16 D. Soren, K. Kumar, P. K. Deheri and P. Pattojoshi, One-pot synthesis of AC/ZnO nanocomposites for highly sensitive, repeatable and fast response humidity sensor, *Ceram. Int.*, 2024, **50**(17), 30422–30433.
17 M. V. Arularasu, Biosynthesis, structural characterization and humidity sensing properties of cellulose/ZnO nanocomposite, *Sens. Bio-Sens. Res.*, 2024, **45**, 100673.
18 M. Rahim, R. Ullah, R. Khattak and I. Rahim, Synthesis, characterization, and humidity sensing performance of polyaniline bismuth-doped zinc oxide (PANI-Bi-ZnO) composites, *Polym. Bull.*, 2024, **81**, 13207–13226.
19 A. Ibrahim, M. A. E. Aal and H. A. Ezzat, Functionalized graphene quantum dots with ZnO as a humidity sensor, *Opt. Quant. Electron.*, 2024, **56**(3), 467.
20 W. F. Yanto, A. Q. Salim, K. Lathifah, A. D. Rohman, A. R. Suryadi, *et al.*, Humidity sensors based on doped ZnO: An overview, *Mater. Today: Proc.*, 2024, DOI: **10.1016/j.matpr.2024.03.049**.
21 A. Mansoori, S. Ahmad, S. Bansal and M. Vashishath, Flexible Graphite-Based Humidity Sensor Using Green Technology, *ECS Sens. Plus*, 2022, **1**(4), 044401.
22 T. F. Choo, K. Y. Kok, N. U. Saidin and N. Mat Zali, Effect of chemical treatment and intrinsic resistance on the humidity sensitivity of pencil graphite sensing material coated on paper substrate, *Sens. Actuators, A*, 2021, **332**, 113085.
23 A. S. Thakur, V. Srivastava and R. Vaish, Pencil drawn interdigitated capacitive sensors on wood substrate, *Adv. Sens. Energy Mater.*, 2024, **3**(4), 100103.
24 A. Erol, S. Okur, B. Comba, Ö. Mermer and M. Ç. Arıkan, Humidity sensing properties of ZnO nanoparticles synthesized by sol–gel process, *Sens. Actuators, B*, 2010, **145**(1), 174–180.
25 R. H. Stokes and R. A. Robinson, Standard Solutions for Humidity Control at 25 °C, *Ind. Eng. Chem.*, 1949, **41**(9), 2013.
26 P. W. Winston and D. H. Bates, Saturated Solutions For the Control of Humidity in Biological Research, *Ecology*, 1960, **41**(1), 232–237.
27 N. I. Sonil, Z. Ullah, S. Haider and W. Ahmad, Flexible UV photodetector based on graphite/titanium dioxide through facile transfer of pencil drawn graphite films on desired substrates, *Ceram. Int.*, 2024, **50**(19), 37057–37066.
28 C. R. Mendes, G. Dilarri, C. F. Forsan, V. d. M. R. Sapata, P. R. M. Lopes, P. B. de Moraes, *et al.*, Antibacterial action and target mechanisms of zinc oxide nanoparticles against bacterial pathogens, *Sci. Rep.*, 2022, **12**(1), 2658.
29 H. Jeong, Y. Noh and D. Lee, Highly stable and sensitive resistive flexible humidity sensors by means of roll-to-roll printed electrodes and flower-like TiO_2 nanostructures, *Ceram. Int.*, 2019, **45**(1), 985–992.
30 I. E. Uflyand, V. A. Zhinzhilo, G. D. Kugabaeva, K. K. Kydralieva and G. I. Dzhardimalieva, Synthesis of nickel-containing metal-polymer nanocomposites and their use as a humidity sensor, *Synth. Met.*, 2024, **307**, 117709.
31 B. Kalim, M. T. Ansar, Z. Ullah, S. K. Abbas, S. Riaz, S. A. Siddiqi, *et al.*, CNTs/ZnO and CNTs/ZnO/Ag multilayers spray coated on cellulose fiber for use as an efficient humidity sensor, *Ceram. Int.*, 2020, **46**(16), 25593–25597.
32 Z.-C. Chen, T.-L. Chang, K.-W. Su, H.-S. Lee and J.-C. Wang, Application of self-heating graphene reinforced polyvinyl alcohol nanowires to high-sensitivity humidity detection, *Sens. Actuators, B*, 2021, **327**, 128934.
33 L. Gong, H. Fu, L. Liu, Z. Li, J. Guo, Z. Cao, *et al.*, Construction and Performance of a Nanocellulose–Graphene-Based Humidity Sensor with a Fast Response and Excellent Stability, *ACS Appl. Polym. Mater.*, 2022, **4**(5), 3656–3666.
34 G. Chaloeipote, J. Samarnwong, P. Traiwatcharanon, T. Kerdcharoen and C. Wongchoosuk, High-performance resistive humidity sensor based on Ag nanoparticles decorated with graphene quantum dots, *R. Soc. Open Sci.*, 2021, **8**(7), 210407.
35 T. Pan, Z. Yu, F. Huang, H. Yao, G. Hu, C. Tang, *et al.*, Flexible Humidity Sensor with High Sensitivity and Durability for Respiratory Monitoring Using Near-Field Electrohydrodynamic Direct-Writing Method, *ACS Appl. Mater. Interfaces*, 2023, **15**(23), 28248–28257.
36 D. Zhang, J. Tong and B. Xia, Humidity-sensing properties of chemically reduced graphene oxide/polymer nanocomposite film sensor based on layer-by-layer nano self-assembly, *Sens. Actuators, B*, 2014, **197**, 66–72.
37 Z. Lou, D. Wu, K. Bu, T. Xu, Z. Shi, J. Xu, *et al.*, Dual-mode high-sensitivity humidity sensor based on MoS_2/Si

nanowires array heterojunction, *J. Alloys Compd.*, 2017, **726**, 632–637.

38 D. Kuntal, S. Chaudhary, A. B. V. Kiran Kumar, R. Megha, C. V. V. Ramana, Y. T. Ravi Kiran, *et al.*, rGO/ZnO nanorods/Cu based nanocomposite having flower shaped morphology: AC conductivity and humidity sensing response studies at room temperature, *J. Mater. Sci.: Mater. Electron.*, 2019, **30**(16), 15544–15552.

39 H. M. M. U. Rehman, A. P. S. Prasanna, M. M. Rehman, M. Khan, S.-J. Kim and W. Y. Kim, Edible rice paper-based multifunctional humidity sensor powered by triboelectricity, *Sustainable Mater. Technol.*, 2023, **36**, e00596.

40 N. A. M. Tahir, S. Liza, K. Fukuda, Y. Yaakob, N. A. Zulkifli, N. A. M. Rawian, *et al.*, Influence of humidity on the tribological performance of graphite reinforced aluminium anodic oxide coating, *Tribol. Int.*, 2024, **197**, 109752.

41 A. Dutta, A. Nirmale, R. Nayak, M. Selvakumar, S. Bhat, S. Paramasivam, *et al.*, Geometric design optimization of polyaniline/graphite nanocomposite based flexible humidity sensor for contactless sensing and breath monitoring, *Mater. Lett.*, 2022, **323**, 132577.

42 Y. Nie, D. Li, Y. Peng, S. Wang, S. Hu, M. Liu, *et al.*, Metal organic framework coated MnO2 nanosheets delivering doxorubicin and self-activated DNAzyme for chemo-gene combinatorial treatment of cancer, *Int. J. Pharm.*, 2020, **585**, 119513.

43 K. Wang, A. Boonpratatong, W. Chen, L. Ren, G. Wei, Z. Qian, *et al.*, The Fundamental Property of Human Leg During Walking: Linearity and Nonlinearity, *IEEE Trans. Neural Syst. Rehabil. Eng.*, 2023, **31**, 4871–4881.

44 R. Zhang, M. Wang, T. Zhu, Z. Wan, X. Chen and X. Xiao, Wireless charging flexible in-situ optical sensing for food monitoring, *Chem. Eng. J.*, 2024, **488**, 150808.